applied optics

Modular-assembled laser system for a long-baseline atom interferometer

Rundong Xu,[1,2] Qi Wang,[1,2] Sitong Yan,[1,2] Zhuo Hou,[1,2] Chuan He,[1,2] Yuhang Ji,[1,2] Zhixin Li,[1,2] Junjie Jiang,[1,2] Biyan Qiao,[1] Lin Zhou,[1,*] Ji Wang,[1,3] and Mingsheng Zhan[1,3,4]

[1]State Key Laboratory of Magnetic Resonance and Atomic and Molecular Physics, Wuhan Institute of Physics and Mathematics, Innovation Academy for Precision Measurement Science and Technology, Chinese Academy of Sciences, Wuhan 430071, China
[2]School of Physical Sciences, University of Chinese Academy of Sciences, Beijing 100049, China
[3]Wuhan Institute of Quantum Technology, Wuhan 430206, China
[4]e-mail: mszhan@wipm.ac.cn
*Corresponding author: lzhou@wipm.ac.cn

Received 15 March 2022; revised 23 April 2022; accepted 3 May 2022; posted 5 May 2022; published 23 May 2022

The Zhaoshan long-baseline Atom Interferometer Gravitation Antenna (ZAIGA) is a new, to the best of our knowledge, type of large-scale atom interferometer facility under construction for the study of gravitation and related problems. To meet the different requirements of the laser system for the atom interferometer using various atoms (including ^{85}Rb, ^{87}Rb, ^{87}Sr, and ^{88}Sr), we design and implement a modular assembled laser system. By dividing the laser system into different basic units according to their functions and modularizing each unit, the laser system is made highly scalable while being compact and stable. Its intensity stability is better than 0.1% in 10^2 s and 0.5% in 10^4 s. We test the performance of the laser system with two experimental systems, i.e., an ^{85}Rb − ^{87}Rb dual-species ultracold atom source and an ^{85}Rb atom interferometer. The ^{85}Rb − ^{87}Rb dual-species magneto-optical trap and the ^{85}Rb atom interference fringes are realized by using this laser system, indicating that its technical performance can meet the major experimental requirements.

https://doi.org/10.1364/AO.458361

1. INTRODUCTION

In recent years, atom interferometers have been widely studied and applied in many fields, such as gravity measurements [1–4], gravity gradient measurements [5,6], rotation measurements [7,8], and fundamental physics [9–19]. The Zhaoshan long-baseline Atom Interferometer Gravitation Antenna (ZAIGA) [19] is a new type of atom interferometer facility proposed for gravitational fundamental research such as gravitational wave detection, gravitational redshift measurement, and the equivalence principle test. One of the key equipment of ZAIGA is the long-baseline atom interferometer (AI). Lasers are important in AIs. Different AI-based experiments have different requirements for laser systems. Experimental setups to study new physics need to achieve more powerful functions, so their laser systems become more complex, and because of the exploratory nature of the experiments, they also need to have good scalability to deal with new requirements. AI systems for applied research need to adapt to changing environmental conditions and meet the requirements of long-term stable measurement. Their laser systems are developing along a simpler and more reliable direction. On the other hand, the AI-based precision measurement experiments [9–18,20–22] are exploratory studies pursuing high precision, and the experimental setup needs good scalability and long-term stability. Currently, traditional laser systems built on optical platforms have good scalability, but are bulk, difficult to move, and susceptible to temperature fluctuations and electromagnetic noise. To overcome the shortcomings of traditional laser systems, some improvement methods have been proposed. First, reducing the free-space light to increase stability, for example, by using the compact fiber modules [23–26] to simplify the complexity of the laser system while avoiding the impact on the optical path due to mechanical problems or other reasons. Second, miniaturization schemes [3,4,27–31] are used to enhance the stability and reduce the size of the mechanical structure, which can be achieved by using an integrated mechanical design and special materials (e.g., Zerodur [25]). In addition, to reduce the influence of the external environment, active or passive vibration isolation, temperature stabilization, and electromagnetic shielding and so on are adopted.

In the ZAIGA facility, a variety of instruments are required to maintain long-term continuous and stable measurements. There are mature instruments such as atom gravimeters, and exploratory instruments such as hundred-meter scale long-baseline atom interferometer in design, in which four species atoms—^{85}Rb, ^{87}Rb, ^{87}Sr, and ^{88}Sr—are included, requiring the

use of different laser wavelengths. Therefore, the laser system in ZAIGA is very complex and needs to be capable of functional expansion and improvement while maintaining long-term stability and reliability. To meet these challenges, we here develop a modular-assembled laser system that can balance stability and scalability. We design the optical modules according to different functions, and each module adopts the design schemes of our mature transportable instruments [3,31]. In addition, independent temperature control and vibration isolation can be implemented for modules to increase their stability. We use polarization-maintaining fibers to integrate different modules into a unit, and this approach makes the entire laser system well scalable. In order to mitigate stability reduction caused by fibers, we take various actions, including temperature control and vibration isolation for the fibers vulnerable to the environment, and laser intensity stabilization techniques. By combining different optical modules, we establish the laser system for the long-baseline atom interferometer. We test its performance by applying it in the $^{85}Rb - {}^{87}Rb$ dual-species ultracold atom source and the ^{85}Rb atom absolute gravimeter.

2. LASER SYSTEM DESIGN

We adopt the following design scheme. First, we divide modules into universal modules and dedicated modules according to functions. By refining the universal optical functions, we design four kinds of universal modules—frequency stabilization seed laser module, power amplification module, acousto-optic frequency shift module, and beam combining and splitting module. For special requirements of each experiment, the Raman laser module, multi-pass acousto-optic frequency shift module, laser time-division multiplexing module, and other modules are designed. Through flexible combination of modules with different functions, requirements of various complex laser systems can be met. Second, each module has various working modes. By changing functional interfaces and reserving extension space, it can adapt to different experimental systems, and maintain the scalability of functions. Modules of the same type have the same standard, which makes it easy to replace the faulted module with a backup. This maintainability is very important to guarantee a continuous operation of such a complex and large device as the long-baseline atom interferometer. Third, the stability of the laser system is further improved by an instrument-level design, temperature control, and vibration isolation for each optical module. In addition, the discrete module design facilitates the elimination of ground loops, and the integrated metal housing can weaken the influence of spatial stray electromagnetic fields.

Unlike transportable instruments, laser systems within the facility prioritize high performance and reliability. Depending on the experimental conditions, the modules can be mounted on cabinets or optical tables. The stability is further enhanced using monitoring and feedback mechanisms: the laser power and frequency are monitored in real time using a photodetector and a Fabry–Perot cavity, respectively, and the laser power is stabilized by feedback adjusting the RF power of an acousto-optic modulator (AOM).

A. Frequency Stabilization of the Seed Laser Module

The seed laser module provides a frequency-locked seed reference laser for the entire laser system. We previously designed an all-AOM laser system [32] to minimize the number of frequency-locked lasers to improve the stability. This scheme also has good scalability, such as by reducing the linewidth of the seed laser, the linewidth of all lasers will be reduced simultaneously. We continue to adopt this scheme and make the seed laser module compatible with multiple frequency locking methods, including optical phase-locked loop, polarization spectroscopy, and modulation transfer spectroscopy.

The schematic of the seed laser module is shown in Figs. 1(a) and 1(b), and the optical structure is a double-sided configuration [31]. We use an external cavity diode laser (Toptica Photonics DL pro) with a linewidth of around 100 kHz to provide the seed laser. To make the optical module more compact and improve its stability, we use small-sized optics (12.7–25.4 mm) and most of the optical mounts (e.g., for wave plate, lens, mirror, isolator) are homemade with the size of 30–50 mm, and the above optical components are common throughout the optical system. In part (a), the beam emitting from a diode laser passes through the isolator and is split into two paths by the polarization beam splitter (PBS). The beam out 1 is coupled into an optical fiber and used in the subsequent experimental process, such as an incident seed laser for the tapered amplifier (TA). Another beam is again divided into two parts: the beam out 2 is coupled into a fiber and transmitted to part (b), and the remaining beam is combined with the incident laser in 1. The combined beam can be injected into a homemade photodetector to obtain the signal used in the beat frequency phase-locked loop or coupled into the fiber from port out 3. To increase polarization stability, there is a half-wave plate in front of all the fiber ports, which is used to adjust the polarization to match the fibers. In part (b), two alternative frequency locking methods are integrated. The example in the figure is the modulation transfer spectroscopy frequency stabilization, where the laser transmitted from part (a) is injected into the module to get the locking signal, and the polarization spectroscopy frequency stabilization [33] can be obtained by a simple modification of optical components. To improve the stability of frequency locking, the laser beam is first filtered by the combination of half-wave plate and PBS, which can make the laser beam with a better linear polarization. In addition, the absorption cell is magnetically shielded to prevent the influence of stray magnetic fields. When the locking signal is obtained, we transfer it to the controller of DL pro and complete the frequency locking by using the lock-in function. The module has the dimensions of 47 cm × 27 cm × 9 cm, and to reduce the size and increase the stability, the optical mounts are the same as that we used in the transportable instrument [31].

B. Power Amplification Module

The power amplification module is used to amplify the seed laser and couple it into different fibers. Taking the commonly used rubidium 780 nm laser as an example, injecting 10–30 mW of seed laser into the TA can obtain 1–2 W of output power. We integrate two TAs into a single module for different application requirements: each TA can be used individually, such as for

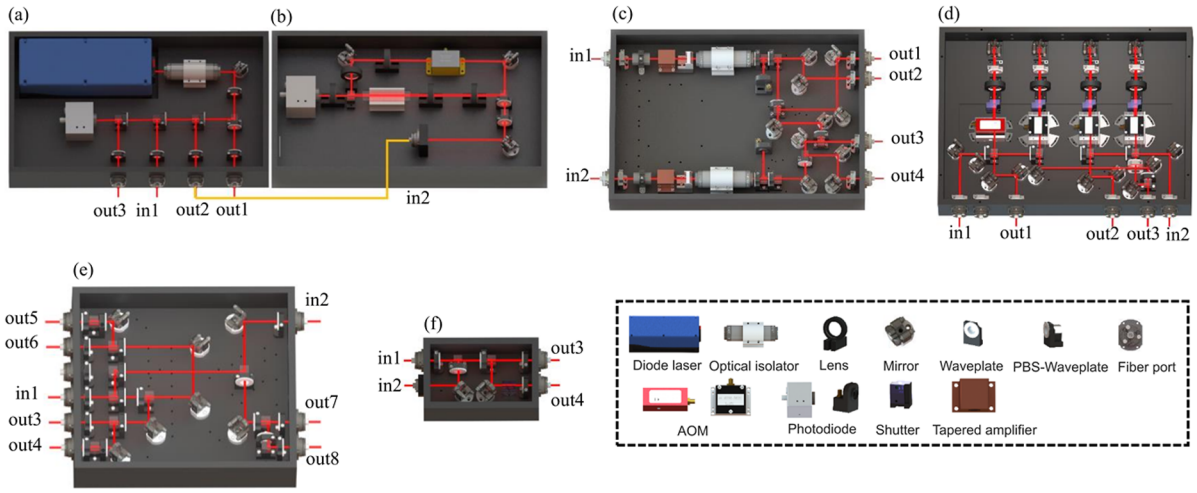

Fig. 1. Optical modules. (a), (b) Seed laser module; (c) power amplification module; (d) acousto-optic frequency shift module; (e), (f) beam splitting and combining module.

cooling or repump lasers, or two TAs are used together, such as for Raman lasers. In order to improve laser utilization efficiency, the laser power can be controlled more flexibly by installing a liquid crystal variable retarder (LCVR, Thorlabs LCC1411) in front of the PBS, so that a time-division multiplexing of high-power lasers can also be realized. For example, in subsequent experiments, Raman lasers are needed for atom interferometer experiments. The LCVR can be installed at an appropriate location before the PBS, such as the laser exit position of the tapered amplifier shown in Fig. 1(c). Since cooling lasers and Raman lasers are not used simultaneously, when the laser emitted from the TA is finished being used as cooling lasers, it can be used as Raman lasers after changing the optical path by controlling the phase of the LCVR. In this way, the utilization efficiency of the laser is increased, and the laser system is made more compact. Figure 1(c) shows the schematic of the power amplification module with a dimension of 45 cm × 32 cm × 6 cm. To make the module more compact, the tapered amplifier is homemade based on the gain chip (Eagleyard, EYP-TPA-0780-02000) with a maximum output power of 2 W; the current controller is Thorlabs-LDC8040 and the temperature controller is Thorlabs-TED8040. Besides power amplification, the TA is insensitive to the power fluctuations of the incident laser within a certain range, which can improve the stability of the optical power.

C. Acousto-Optic Frequency Shift Module

The acousto-optic frequency shift module has functions of frequency shifting, switching, beam splitting and combining, and power stabilization. According to different requirements of the experiment, a single beam laser can be shifted independently such as the detection laser, or split and shifted separately and then combined, such as double diffraction Raman lasers. Two beams can be shifted separately and then combined, such as a cooling laser and a repump laser. Our acousto-optic frequency shift module has these three different application modes and only a few of the optical components need to be replaced to achieve a variety of frequency shifting functions.

A typical application of this module is shown in Fig. 1(d): two incident beams, in 1 and in 2, are split and double-pass the AOMs (AA Opto-Electronic, 80–350 MHz) to obtain four beams with controllable frequency and power, two of which exit independently, and the others are first combined and then exit. The AOM is mounted on a homemade aluminum base, which is compact, mechanically stable, and has good thermal conductivity, and also allows the position of the AOM to be adjusted in both horizontal and vertical directions to obtain the best diffraction efficiency. In this way, the diffraction efficiency of the +1st order (−1st order) laser beam is greater than 80%. All component positions in the frequency shift module are strictly optimized. When the components are installed, only fine adjustments are needed to achieve high diffraction and coupling efficiencies, which greatly reduces the difficulty of adjustment. In addition, a homemade shutter [34] is installed after each AOM to realize the complete shutdown of the laser, and the size of the module is 45 cm × 33 cm × 6 cm.

D. Beam Splitting and Combining Module

In laser systems, it is often necessary to combine and split the laser beams by coupling multiple frequency lasers into one or more fibers or coupling one laser to multiple fibers. The former is more often used for manipulation of the atomic state, and the latter is mostly used for the preparation of cold atom sources. It is also necessary to control the switching and power of the laser beam. We design two types of beam splitting and combining modules. Module 1 shown in Fig. 1(f) can realize beam splitting or combining. For relatively simple requirements, one or more such modules can be combined. More complex applications can be achieved with module 2 through different installation schemes, as shown in Fig. 1(e). A laser shutter can be installed at an appropriate position, and the half-wave plate can be replaced with a LCVR for more flexible control of the laser power distribution. In both kinds of modules, the power of each outgoing laser beam is adjustable, which is necessary for many experiments. Since these modules are relatively small, they can be placed close to the vacuum system, so that the outgoing

beam can be coupled into the optical fiber with short length and good polarization-maintaining performance, which can increase the polarization stability. Module 1 has the dimensions of 17 cm × 11 cm × 6 cm, and module 2 has the dimensions of 31 cm × 28 cm × 6 cm.

E. Dedicated Module

Universal optical modules can be used in different experimental systems, and according to specific requirements, we develop some dedicated modules, including the multi-pass acousto-optic frequency shift module [35], laser time-division multiplexing system [18,36], and Raman laser module [37], which are complementary to the universal modules.

The multi-pass acousto-optic frequency shift module is based on a 350 MHz AOM, which can realize 4-, 6-, 8-, and 12-pass acousto-optic frequency shift up to 5 GHz, maintaining a diffraction efficiency of nearly 8%. The eight-pass acousto-optic frequency shift module can achieve a laser output with a frequency shift of 2.8 GHz, diffraction efficiency of 20%, and output power above 30 mW, which can be directly used as a seed laser of the TA.

The time-division multiplexing system can realize fast switching of lasers with different frequencies, so that lasers can be efficiently used in different experimental periods. It is often used in combination with Raman lasers, state preparation lasers, and detection lasers, where the extinction ratio between different lasers is better than 30 dB, and the switching time is in the 100 ns level. The Raman laser module uses a high-frequency AOM to generate high-quality Raman lasers for atom interferometer experiments.

F. Auxiliary Modules

To meet the requirements of transportable and long-term stable operation of the laser system, auxiliary modules are also required, such as movable cabinets, an environmental monitoring system, and a temperature feedback system.

In the absence of an optical table, all optical modules can be installed in a cabinet assembled from aluminum alloy profiles with wheels at the bottom. Temperature and humidity sensors are installed in the cabinet to monitor environmental conditions in real-time. There are many heat-generating devices in optical systems, such as AOMs and TAs. The heat generated by these devices can change the thermal distribution within the module, resulting in mechanical thermal deformation, affecting the fiber coupling efficiency of the laser, and causing power instability. The performance of these devices is also affected if the ambient temperature changes or if the heat generated by themselves cannot be dissipated quickly. Therefore, it is necessary to control the temperature of the module containing the heat-generating devices. We use polyimide thermofoil heaters, thermistors, power supplies, and feedback control circuits to actively control the temperature. Since temperature fluctuations can also affect the polarization-maintaining performance of fibers, we also use the method of thermal insulation to control the temperature of fibers to enhance the polarization stability. Electronic devices, such as laser controllers, TA controllers, and signal sources, are installed in another cabinet to make the entire laser system more compact and easier to move.

3. LASER SYSTEM PERFORMANCE

Due to the all-AOM frequency shifting scheme [36], the final frequency stability of the entire laser system is mainly determined by the frequency-locked laser. The polarization stability is ultimately determined by the outgoing polarization-maintaining fibers, and since the laser often passes through the PBS before interacting with atoms, the polarization stability is reflected in the stability of intensity. In precision measurement experiments, the fluctuation of laser intensity affects the long-term stability and accuracy of the measurement. Ensuring the stability of the laser intensity is a major challenge of this laser system. In this paper, we focus on evaluating the performance of this laser system by measuring its intensity stability. Discrete modules increase flexibility, but also increase laser power loss. The largest loss occurs when coupling the free-space laser beams into the fibers. We match the incident laser beams by using fiber couplers with different mode field diameters to achieve the best coupling efficiency. For TAs, we achieve a coupling efficiency of more than 60%. For other free-space laser beams, the coupling efficiency is above 80%.

In our equivalence principle test experiment in 2015, the maximum fluctuation of laser intensity was 10% [18], which then decreased to 2% [38], and the initial goal of ZAGAI is to control the fluctuation to less than 1%. To minimize the fluctuation of laser intensity, we first improve the stability of the laser polarization. Before entering the fiber, the polarization of the laser is optimized by passing through a high extinction ratio PBS and a combination of the quarter-wave plate and half-wave plate. Second, the fiber with suitable length and the module are combined to improve their adaptability. For example, the splitting module can be placed close to the vacuum system due to its small size, so a shorter fiber with better intensity and polarization stability can be used to export the laser. In addition, the insensitivity of the TA to the intensity fluctuation of the incident laser is exploited to improve the output power stability. As shown in Fig. 2, when the incident seed laser power increases

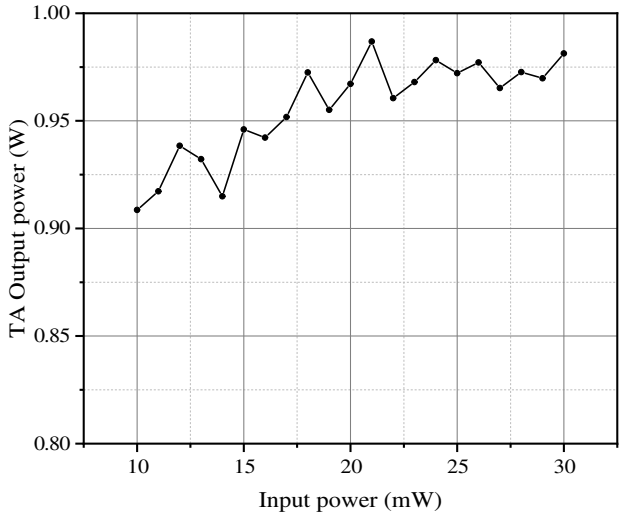

Fig. 2. TA output power at different input powers.

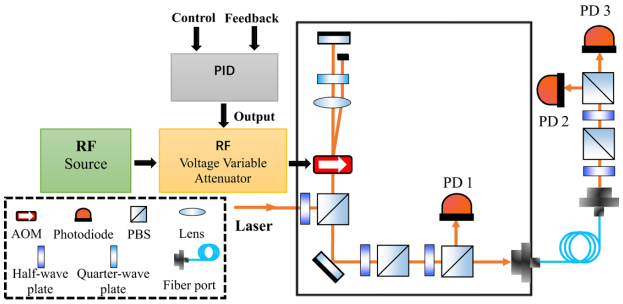

Fig. 3. Laser intensity stability test scheme.

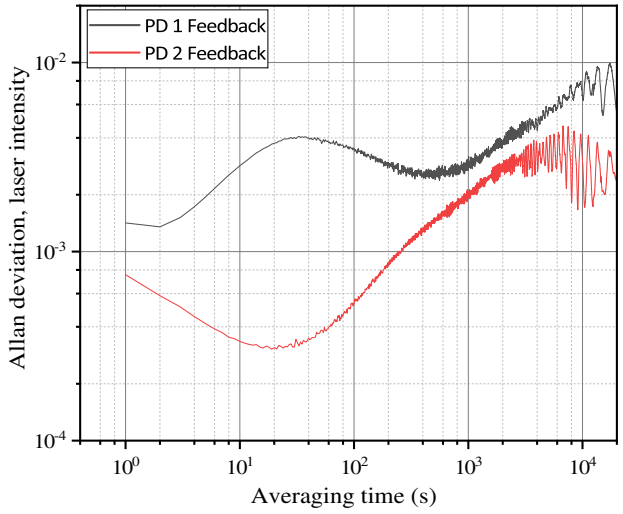

Fig. 4. Allan deviation of laser intensity stability (normalized to average value). The laser intensity is detected by PD 3. PD 1 as the feedback signal (black solid line) and PD 2 as the feedback signal (red solid line).

from 15 to 30 mW, the amplified laser power variation is less than 5%. Based on the above measures, further use of intensity stabilization can improve short-term and long-term stability.

We carry out the stability test on two typical laser intensity locking applications: the locking feedback points are at the input and output ends of the fiber, respectively, which is mainly determined by the laser intensity stability requirements and where it is convenient to establish the feedback point. The RF signal generated by the signal source (RIGOL, DG4162) first passes through the voltage-controlled attenuator (MINI-CIRCUITS, ZX73-2500M), and then is amplified by the power amplifier and applied to the AOM. The power detector converts the optical signal of the diffracted beam into a voltage signal and inputs it to the homemade proportional-integral-differential (PID) circuit. After the detected signal is compared with the reference signal, the difference is calculated by the PID circuit and output to the voltage-controlled attenuator, which changes the intensity of the RF signal applied to the AOM and then changes the intensity of the diffracted beam. This feedback loop enables stabilization and control of the laser power.

The test schematic is shown in Fig. 3, where the outputs of PD 1 and PD 2 are used as feedback signals for locking, respectively, and PD 3 is used for detecting the laser intensity. The results of laser intensity stability (normalized to average value) are shown in Fig. 4. When PD 1 is used as the feedback signal, the intensity stability is better than 0.5% in 10^2 s and 1 % in 10^4 s; when PD 2 is used as the feedback signal, the intensity stability is better than 0.1 % in 10^2 s and 0.5 % in 10^4 s. Thus, the intensity stability of this laser system meets our requirements.

4. APPLICATION OF THE LASER SYSTEM

To verify the performance of this laser system, we apply it in the ^{85}Rb – ^{87}Rb dual-species ultracold atom source and the ^{85}Rb atom interferometer, respectively. The two experimental systems are to be used for the future long-baseline atom interferometer. The ^{85}Rb – ^{87}Rb dual-species magneto-optical trap (MOT) is realized, and the interference fringes of ^{85}Rb are preliminarily obtained.

A. ^{85}Rb – ^{87}Rb Dual-Species Ultracold Atom Source

The ^{85}Rb – ^{87}Rb dual-species ultracold atom source will be used for the equivalence principle test and verification experiment of gravitational wave detection technology. Figure 5 is the schematic diagram of the laser system, which consists of a seed laser module, four TA amplification modules, eight acousto-optic frequency shift modules, five splitting modules, and an eight-pass acousto-optic frequency shift module. It provides different lasers for cooling, trapping, and detection of ^{85}Rb and ^{87}Rb atoms.

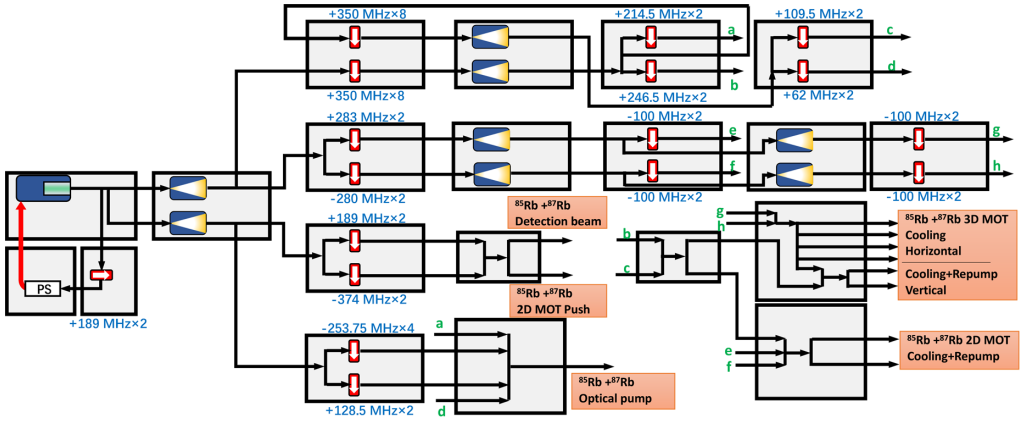

Fig. 5. ^{85}Rb – ^{87}Rb two-component ultracold atom source laser system.

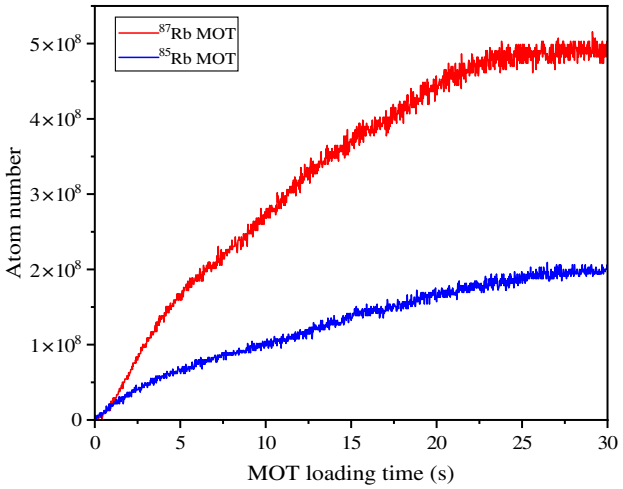

Fig. 6. ^{87}Rb and ^{85}Rb MOT loading curves.

We use this laser system to perform the ^{85}Rb − ^{87}Rb dual-species MOT experiment, where the power of the ^{87}Rb (^{85}Rb) 2D and the 3D cooling laser is 40 (42) mW and 85 (95) mW, and the repump laser power is 20 mW (24 mW). Figure 6 shows the experimental results of the MOT loading curves for ^{87}Rb and ^{85}Rb, and the atom numbers are 5×10^8 for ^{87}Rb and 2×10^8 for ^{85}Rb.

B. ^{85}Rb Atom Interferometer

The ^{85}Rb cold atom interferometer is mainly used for monitoring the background gravity field in the long-baseline atom interferometer. Figure 7 shows the schematic diagram of the cooling laser system, which comprises a seed laser module, a TA module, an eight-pass acousto-optic frequency shift module, four frequency shift modules, and a beam splitting module. The Raman laser module used in the experiment is described in [37]. Figure 8 shows the interference fringes for $T = 100$ ms and the contrast is 18%. The uncertainty of phase is 12.4 mrad, and the resolution of gravity measurement using single fringe is 8 μGal without vibration isolation and noise rejection.

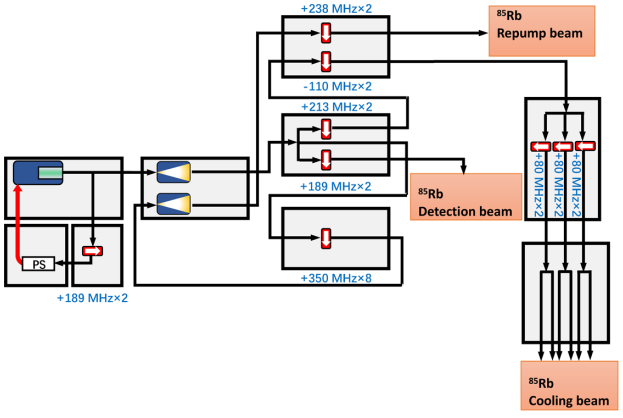

Fig. 7. ^{85}Rb atom interferometer cooling laser system.

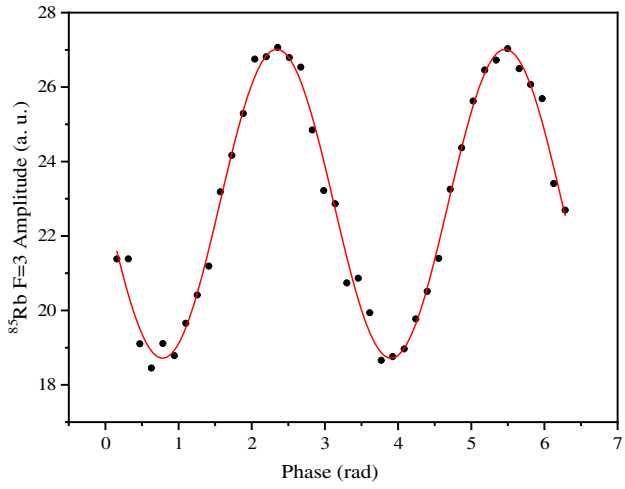

Fig. 8. ^{85}Rb atomic interference fringe for $T = 100$ ms. The black dots are experimental data, and the red solid line is Sine fitting.

5. DISCUSSION AND CONCLUSION

We designed and implemented a laser system for a long-baseline atom interferometer in ZAIGA [19]. The system comprises universal modules, dedicated modules, and auxiliary modules, and it has instrument-level reliability, portability, and scalability. The performance of the laser system can meet our requirements according to the test results. We performed two experiments based on this laser system and obtained the ^{85}Rb − ^{87}Rb dual-species MOT and the ^{85}Rb interference fringe. Because of the modular assembled design scheme, the laser system is highly scalable, and it can also be applied to ^{87}Sr and ^{88}Sr atoms in the future. It provides specific and feasible solutions for high-precision measurements and long-term stable operation of various instruments in the ZAIGA facility.

Funding. National Natural Science Foundation of China (91536221, 12174403, 91736311); National Key Research and Development Program of China (2016YFA0302002); Strategic Priority Research Program of the Chinese Academy of Sciences (XDB21010100); Youth Innovation Promotion Association of the Chinese Academy of Sciences (2016300).

Disclosures. The authors declare no conflicts of interest.

Data availability. Data underlying the results presented in this paper are not publicly available at this time but may be obtained from the authors upon reasonable request.

REFERENCES

1. A. Peters, K. Y. Chung, and S. Chu, "Measurement of gravitational acceleration by dropping atoms," Nature **400**, 849–852 (1999).
2. Z. K. Hu, B. L. Sun, X. C. Duan, M. K. Zhou, L. L. Chen, S. Zhan, Q. Z. Zhang, and J. Luo, "Demonstration of an ultrahigh-sensitivity atom-interferometry absolute gravimeter," Phys. Rev. A **88**, 043610 (2013).
3. P. W. Huang, B. Tang, X. Chen, J. Q. Zhong, Z. Y. Xiong, L. Zhou, J. Wang, and M. S. Zhan, "Accuracy and stability evaluation of the ^{85}Rb atom gravimeter WAG-H5-1 at the 2017 International Comparison of Absolute Gravimeters," Metrologia **56**, 045012 (2019).
4. X. J. Wu, Z. Pagel, B. S. Malek, T. H. Nguyen, F. Zi, D. S. Scheirer, and H. Müller, "Gravity surveys using a mobile atom interferometer," Sci. Adv. **5**, eaax0800 (2019).
5. M. J. Snadden, J. M. McGuirk, P. Bouyer, K. G. Haritos, and M. A. Kasevich, "Measurement of the Earth's gravity gradient with an atom interferometer-based gravity gradiometer," Phys. Rev. Lett. **81**, 971–974 (1998).

6. F. Sorrentino, Q. Bodart, L. Cacciapuoti, Y. H. Lien, M. Prevedelli, G. Rosi, L. Salvi, and G. M. Tino, "Sensitivity limits of a Raman atom interferometer as a gravity gradiometer," Phys. Rev. A **89**, 023607 (2014).
7. B. Canuel, F. Leduc, D. Holleville, A. Gauguet, J. Fils, A. Virdis, A. Clairon, N. Dimarcq, C. J. Bordé, A. Landragin, and P. Bouyer, "Six-axis inertial sensor using cold-atom interferometry," Phys. Rev. Lett. **97**, 010402 (2006).
8. T. L. Gustavson, P. Bouyer, and M. A. Kasevich, "Precision rotation measurements with an atom interferometer gyroscope," Phys. Rev. Lett. **78**, 2046–2049 (1997).
9. P. Asenbaum, C. Overstreet, M. Kim, J. Curti, and M. A. Kasevich, "Atom-interferometric test of the equivalence principle at the 10-12 level," Phys. Rev. Lett. **125**, 191101 (2020).
10. B. Barrett, L. Antoni-Micollier, L. Chichet, B. Battelier, T. Lévèque, A. Landragin, and P. Bouyer, "Dual matter-wave inertial sensors in weightlessness," Nat. Commun. **7**, 13786 (2016).
11. X. C. Duan, X. B. Deng, M. K. Zhou, K. Zhang, W. J. Xu, F. Xiong, Y. Y. Xu, C. G. Shao, J. Luo, and Z. K. Hu, "Test of the universality of free fall with atoms in different spin orientations," Phys. Rev. Lett. **117**, 023001 (2016).
12. S. Fray, C. A. Diez, T. W. Hänsch, and M. Weitz, "Atomic interferometer with amplitude gratings of light and its applications to atom based tests of the equivalence principle," Phys. Rev. Lett. **93**, 240404 (2004).
13. H. Müller, S. W. Chiow, S. Herrmann, S. Chu, and K. Y. Chung, "Atom-interferometry tests of the isotropy of post-Newtonian gravity," Phys. Rev. Lett. **100**, 031101 (2008).
14. R. H. Parker, C. Yu, W. Zhong, B. Estey, and H. Müller, "Measurement of the fine-structure constant as a test of the Standard Model," Science **360**, 191–195 (2018).
15. G. Rosi, F. Sorrentino, L. Cacciapuoti, M. Prevedelli, and G. M. Tino, "Precision measurement of the Newtonian gravitational constant using cold atoms," Nature **510**, 518–521 (2014).
16. D. Schlippert, J. Hartwig, H. Albers, L. L. Richardson, C. Schubert, A. Roura, W. P. Schleich, W. Ertmer, and E. M. Rasel, "Quantum test of the universality of free fall," Phys. Rev. Lett. **112**, 203002 (2014).
17. M. G. Tarallo, T. Mazzoni, N. Poli, D. V. Sutyrin, X. Zhang, and G. M. Tino, "Test of Einstein equivalence principle for 0-spin and half-integer-spin atoms: search for spin-gravity coupling effects," Phys. Rev. Lett. **113**, 023005 (2014).
18. L. Zhou, S. T. Long, B. Tang, X. Chen, F. Gao, W. C. Peng, W. T. Duan, J. Q. Zhong, Z. Y. Xiong, J. Wang, Y. Z. Zhang, and M. S. Zhan, "Test of equivalence principle at 10-8 level by a dual-species double-diffraction Raman atom interferometer," Phys. Rev. Lett. **115**, 013004 (2015).
19. M. S. Zhan, J. Wang, W. T. Ni, *et al.*, "ZAIGA: Zhaoshan long-baseline atom interferometer gravitation antenna," Int. J. Mod. Phys. D **29**, 1940005 (2019).
20. B. Canuel, S. Abend, P. Amaro-Seoane, *et al.*, "ELGAR—a European Laboratory for Gravitation and Atom-interferometric Research," Class. Quantum Gravity **37**, 225017 (2020).
21. B. Canuel, A. Bertoldi, L. Amand, *et al.*, "Exploring gravity with the MIGA large scale atom interferometer," Sci. Rep. **8**, 14064 (2018).
22. J. Hartwig, S. Abend, C. Schubert, D. Schlippert, H. Ahlers, K. Posso-Trujillo, N. Gaaloul, W. Ertmer, and E. M. Rasel, "Testing the universality of free fall with rubidium and ytterbium in a very large baseline atom interferometer," New J. Phys. **17**, 035011 (2015).
23. C. Diboune, N. Zahzam, Y. Bidel, M. Cadoret, and A. Bresson, "Multi-line fiber laser system for cesium and rubidium atom interferometry," Opt. Express **25**, 16898–16906 (2017).
24. F. Lienhart, S. Boussen, O. Carraz, N. Zahzam, Y. Bidel, and A. Bresson, "Compact and robust laser system for rubidium laser cooling based on the frequency doubling of a fiber bench at 1560 nm," Appl. Phys. B **89**, 177–180 (2007).
25. D. O. Sabulsky, J. Junca, G. Lefevre, X. Zou, A. Bertoldi, B. Battelier, M. Prevedelli, G. Stern, J. Santoire, Q. Beaufils, R. Geiger, A. Landragin, B. Desruelle, P. Bouyer, and B. Canuel, "A fibered laser system for the MIGA large scale atom interferometer," Sci. Rep. **10**, 3268 (2020).
26. F. Theron, Y. Bidel, E. Dieu, N. Zahzam, M. Cadoret, and A. Bresson, "Frequency-doubled telecom fiber laser for a cold atom interferometer using optical lattices," Opt. Commun. **393**, 152–155 (2017).
27. S. Merlet, L. Volodimer, M. Lours, and F. Pereira Dos Santos, "A simple laser system for atom interferometry," Appl. Phys. B **117**, 749–754 (2014).
28. V. Schkolnik, O. Hellmig, A. Wenzlawski, J. Grosse, A. Kohfeldt, K. Döringshoff, A. Wicht, P. Windpassinger, K. Sengstock, C. Braxmaier, M. Krutzik, and A. Peters, "A compact and robust diode laser system for atom interferometry on a sounding rocket," Appl. Phys. B **122**, 217 (2016).
29. M. Schmidt, M. Prevedelli, A. Giorgini, G. M. Tino, and A. Peters, "A portable laser system for high-precision atom interferometry experiments," Appl. Phys. B **102**, 11–18 (2011).
30. Q. Y. Wang, Z. Y. Wang, Z. J. Fu, W. Y. Liu, and Q. Lin, "A compact laser system for the cold atom gravimeter," Opt. Commun. **358**, 82–87 (2016).
31. X. W. Zhang, J. Q. Zhong, B. Tang, X. Chen, L. Zhu, P. W. Huang, J. Wang, and M. S. Zhan, "Compact portable laser system for mobile cold atom gravimeters," Appl. Opt. **57**, 6545–6551 (2018).
32. C. He, S. T. Yan, L. Zhou, S. Barthwal, R. D. Xu, C. Zhou, Y. H. Ji, Q. Wang, Z. Hou, J. Wang, and M. S. Zhan, "All acousto-optic modulator laser system for a 12 m fountain-type dual-species atom interferometer," Appl. Opt. **60**, 5258–5265 (2021).
33. W. C. Peng, L. Zhou, S. T. Long, J. Wang, and M. S. Zhan, "Locking laser frequency of up to 40 GHz offset to a reference with a 10 GHz electro-optic modulator," Opt. Lett. **39**, 2998–3001 (2014).
34. P. W. Huang, B. Tang, Z. Y. Xiong, J. Q. Zhong, J. Wang, and M. S. Zhan, "Note: A compact low-vibration high-performance optical shutter for precision measurement experiments," Rev. Sci. Instrum. **89**, 096111 (2018).
35. C. Zhou, C. He, S. T. Yan, Y. H. Ji, L. Zhou, J. Wang, and M. S. Zhan, "Laser frequency shift up to 5 GHz with a high-efficiency 12-pass 350 MHz acousto-optic modulator," Rev. Sci. Instrum. **91**, 033201 (2020).
36. W. Yang, L. Zhou, S. T. Long, W. C. Peng, J. Wang, and M. S. Zhan, "Time-division-multiplexing laser seeded amplification in a tapered amplifier," Chin. Opt. Lett. **13**, 011401 (2015).
37. L. Zhou, Z. Y. Xiong, W. Yang, B. Tang, W. C. Peng, Y. B. Wang, P. Xu, J. Wang, and M. S. Zhan, "Measurement of local gravity via a cold atom interferometer," Chin. Phys. Lett. **28**, 013701 (2011).
38. L. Zhou, C. He, S. T. Yan, X. Chen, D. F. Gao, W. T. Duan, Y. H. Ji, R. D. Xu, B. Tang, C. Zhou, S. Barthwal, Q. Wang, Z. Hou, Z. Y. Xiong, Y. Z. Zhang, M. Liu, W. T. Ni, J. Wang, and M. S. Zhan, "Joint mass-and-energy test of the equivalence principle at the 10-10 level using atoms with specified mass and internal energy," Phys. Rev. A **104**, 022822 (2021).